

A Study of Some Current Methods of Analysing Observations of Star Forming Regions

S. D. Doty & M. L. Palotti

Department of Physics and Astronomy, Denison University, Granville, OH 43023, USA

Accepted 2002 May 13; Received 2002 May 11; in original form 2002 February 13

ABSTRACT

We present an evaluative study of some current methods utilized in the analysis of infrared (IR) observations of star-forming regions. A series of self-consistent radiative transfer models are constructed, with the outputs analysed using these methods to infer source properties such as dust temperature, mass, opacity function, and density distribution. Any discrepancies between the inferred and model quantities can be attributed to the analysis methods. The range of validity of most methods is smaller than expected, due to two effects: (1) limited applicability of the Rayleigh-Jeans limit except to very long wavelengths, and (2) significant errors in the isothermal approximation, even when $\Delta T(r) < 2\text{K}$ over 90 per cent of a region. Still, an accurate mean T_{dust} can be found using a modified Wiens law. This temperature can yield dust masses to within 10-25 per cent – much better than masses inferred from the integrated luminosity. Using long wavelengths ($> 1000 - 2000\mu\text{m}$), the opacity index can be determined from the far-IR spectrum to within 20 per cent. Fitting the spectrum yields better results. The density distribution can be somewhat constrained by fitting the surface brightness, for well-resolved sources. Better results are found by fitting the flux spectrum with detailed models.

Key words: stars: formation – infrared: stars – ISM: clouds.

1 INTRODUCTION

Infrared (IR) radiation, due to thermal emission from dust grains, is a key feature of star-forming regions. These grains play an important role in the chemistry, thermal balance, and evolution of these regions. This role, coupled with the ability for IR radiation to escape from areas of high optical depth, makes the determination of source parameters through the study of IR observations of great importance.

The problem of obtaining source parameters from the IR observations is a difficult one. As a result, it is important to study and evaluate the analysis methods used to judge their value and regimes of validity.

In general, the analysis of IR observations can be broadly broken into two groups. The first approach relies upon the use of relatively simple, semi-analytic expressions which are derived from idealized and simplified approximations and assumptions (see e.g. Hildebrand 1983). It has been shown previously that the strict use of this approach may lead to interpretations which are ambiguous or erroneous (see e.g., Schmid-Bergk & Scholz 1976; Butner et al. 1991; Doty & Leung 1994; Men'shchikov & Henning 1997; Shirley, et al. 2000). The second approach involves the construction (usually a grid) of detailed, self-consistent radiative transfer models for the computation of model spec-

tra and comparison with observations. While such codes are available for use by the general community (e.g. CS-DUST3 by Egan, Leung, & Spagna 1983; DUSTY by Ivezić, Nenkova, & Elitzur 1999), constructing such models requires substantial time and effort. As a result, the first approach remains a common choice.

In this paper we critically evaluate semi-analytic methods of analysis of IR observations of star-forming regions. Here we consider internal and externally heated dust clouds as analogues of early-type star-forming regions. In particular, we examine the usual assumptions of homogeneities in density and temperature, as well as the neglect of opacity effects when applied to externally heated IR sources. We do this by constructing a series of realistic models of these regions, treating the model output as simulated observations. We then apply common semi-analytic methods to infer the source properties, and compare them to those used in constructing the models. The discrepancies between the input and inferred source properties yield a measure of the limitations of the semi-analytic methods used.

The outline of this paper is as follows. In Section 2 we summarize the problem and current methods of analysis. We describe the models run and testing procedure in Section 3. In Section 4, we discuss the role and determination of the dust temperature. We consider the dust mass in Section 5.

In Section 6 we discuss the determination of the dust opacity function. We consider the determination of the dust density distribution in Section 7. Finally, in Section 8, we summarize and draw conclusions from this study.

2 ANALYTICAL DESCRIPTION OF THE PROBLEM AND SUMMARY OF SOME CURRENT METHODS OF ANALYSIS

2.1 Emergent radiation

For a spherically symmetric dust shell, the specific luminosity, defined to be the amount of energy emitted per unit frequency per unit time can be written as

$$L_\nu = \int \langle Q_a \pi a^2 \rangle_\nu B_\nu[T(r)] e^{-\tau(\nu,r)} n(r) 4\pi r^2 dr. \quad (1)$$

Here $B_\nu[T(r)]$ is the Planck function at the dust temperature, $T(r)$, and τ_ν , $\langle Q_a \pi a^2 \rangle_\nu$, and $n(r)$ are the optical depth, grain absorption coefficient, and density distribution respectively as defined below. The density distribution and the grain absorption cross section are both assumed to be power laws with indices m and β , given by

$$n(r) = n_0 (r_0/r)^m, \quad (2)$$

and

$$Q_\nu \equiv \langle Q_a \pi a^2 \rangle_\nu = Q_0 (\nu/\nu_0)^\beta, \quad (3)$$

respectively. The optical depth, τ_ν , at a radius r is defined as

$$\tau_\nu = \int Q_\nu n(r) dr. \quad (4)$$

For convenience, we define the optical depth in the visible to be $\tau_0 \equiv \tau_{0.55\mu\text{m}}$.

In order to evaluate the specific luminosity explicitly, the temperature distribution, $T(r)$, density distribution, and grain properties need to be known. For this reason, it is common to assume that sources are isothermal and optically thin. In this limit, equation (1) simplifies to

$$L_\nu = Q_\nu B_\nu(T) \int n(r) 4\pi r^2 dr = Q_\nu B_\nu(T) \frac{M_{\text{dust}}}{m_{\text{grain}}}, \quad (5)$$

and can then be solved analytically if the density distribution is known or assumed to be known. From equation (5) we can derive semi-analytic expressions for many of the source parameters, as discussed below.

2.2 Dust temperature

As stated above, it is common to assume that sources are isothermal (see, e.g., Launhardt et al. 1996). In order to determine the temperature of such a source, Wiens law denoting the peak of an unmodified blackbody spectrum (B_ν) is often used (assuming an isothermal source as in eq. [5]),

$$T = \frac{2898}{\lambda_{\text{peak}}(\mu\text{m})} \text{K}. \quad (6)$$

It is also possible to find the temperature by fitting the flux spectrum (see Sect 2.4). In practice this takes many forms, depending upon the quantity and quality of data available for a given source. These approaches range from fitting the

observed flux at a single wavelength point to find a single equivalent brightness temperature (e.g. Henning et al. 2000), to using a two-wavelength effective color temperature (e.g. Grady et al. 2001) to fitting the flux spectrum with a single temperature greybody (e.g., Siebenmorgen, Krügel, & Chini 1999), to using two temperature components (e.g., Krügel et al. 1998; Ward-Thompson et al. 2000). In many cases, the dust properties are assumed to be known *a priori* (e.g., Krügel et al. 1998; Henning et al. 2000), though they are sometimes determined directly from the observations (see e.g., Launhardt, Ward-Thompson, & Henning 1997; Voshchinnikov & Krügel 1999; Abraham et al. 2000; and Sect 2.4).

2.3 Dust mass

Assuming a dust grain mass m_{grain} , the total dust mass of the source is

$$M_{\text{dust}} = m_{\text{grain}} \int n(r) 4\pi r^2 dr. \quad (7)$$

In the optically thin and isothermal limits, the dust mass can be expressed in terms of the specific luminosity (see eq. [5]) by

$$M_{\text{dust}} = (m_{\text{grain}} L_\nu) / (B_\nu Q_\nu). \quad (8)$$

By expressing the specific luminosity in terms of the observed flux, $f_{\nu,\text{obs}}$, and the distance to the source, D , the mass can be written as

$$M_{\text{dust}} = (m_{\text{grain}} f_{\nu,\text{obs}} D^2) / (B_\nu Q_\nu) \quad (9)$$

(Hildebrand 1983; in various forms by, e.g. Beichman et al. 1990, Launhardt et al. 1996; Siebenmorgen, Krügel, & Chini 1999). As can be seen, the dust mass can be determined from the observed flux and an estimate of the distance to the source. Unfortunately, this requires a good estimate of both the dust temperature (see Sect. 4) and grain opacity function (see Sect. 6) for an accurate dust mass estimate.

The mass of the dust can also be determined by the spectral energy distribution (Doty and Leung 1994). The energy emitted from the dust is simply a reprocessing of the energy that the dust has absorbed. As a result, in an optically thin source the total emission is related to the total amount absorbed, which varies with optical depth or dust mass.

$$L \equiv \int L_\nu d\nu \propto M, \quad (10)$$

assuming that the temperature is not a function of the dust mass.

2.4 Grain opacity function

For an optically thin source and when the Rayleigh Jeans approximation ($h\nu \ll kT$; RJA) holds, the specific luminosity becomes

$$L_\nu \propto \nu^{2+\beta} \int T(r) n(r) 4\pi r^2 dr. \quad (11)$$

By taking the ratio of luminosities at two different frequencies, the opacity index, β can be determined (Helou 1989) as

$$\beta = [\log(L_{\nu 1}/L_{\nu 2})/\log(\nu_1/\nu_2)] - 2. \quad (12)$$

An interesting predictor-corrector-like iteration method was utilized by Siebenmorgen, Krügel, & Chini (1999). In this approach, previous greybody models of similar sources were used to guess a single dust temperature. This was used to infer a dust opacity index, β . Given this value of β the data were fit to find T . Finally, the corrected value dust temperature was used to find a final value for β . While each step of the iteration used methods/assumptions described elsewhere here, the iterative approach helped to break the degeneracy between temperature and dust opacity.

On the other hand, given the power of modern computers, and the large amounts of high quality far-infrared and submillimeter data becoming available for many sources, it is possible to consider the coupled problem and determine the temperature and the opacity index by fitting the observed spectrum (see, e.g., Krugel et. al. 1998; Ward-Thompson et al. 2000; Abraham et al. 2000). For an isothermal, optically thin source, the specific luminosity can be written as

$$L_{\nu} = a_1 \nu^{a_3} B_{\nu}(a_2), \quad (13)$$

where a_1 , a_2 , and a_3 become fitting parameters. Here, the density distribution is incorporated into a_1 , the temperature is a_2 , and the opacity index, β , is a_3 . To compute values for the fitting parameters, the chi-squared

$$\chi^2 = \sum [y_{\text{actual}}(i) - y_{\text{fit}}(i)]^2 / \sigma^2(i), \quad (14)$$

is minimized for a given set of frequencies. The uncertainty in the measure of luminosity ($y(i)$) is defined by the parameter $\sigma(i)$. We have only considered the case where the uncertainty is equal to a small fraction of $y(i)$ (Doty and Leung 1994). This has the effect of equally weighting each point in the spectrum.

2.5 Dust density distribution index

If a resolved source is assumed to be isothermal along any line of sight, the mean intensity can be written as

$$I_{\nu} = \tau_{\nu} B_{\nu}. \quad (15)$$

Adopting a power law form for the optical depth, $\tau_{\nu} \propto Q_{\nu} \propto \nu^{\beta}$, and taking the ratio at two different frequencies, equation (15) is then

$$\frac{I_{\nu 1}}{I_{\nu 2}} = \frac{\nu_1^{\beta} B_{\nu 1}}{\nu_2^{\beta} B_{\nu 2}} \quad (16)$$

Assuming that the optical index, β , is known (see Sect. 6), a temperature can be found given a ratio of intensities. Using this temperature in equation (15) will yield the optical depth for that frequency and line of sight. The optical depth at a given impact parameter is related to the column density, N , along that line of sight. Therefore, the form of the optical depth map will be the same form as a column density map for the same source. Finally, the power law form for the column density, $N(r) \propto r^{-\alpha}$, can be related to the power law form of the density distribution, $n(r) \propto r^{-m}$ (Tomita et al. 1979) where $m = 1 + \alpha$. As Yun and Clemens (1991) point out, however, this is only appropriate for an infinite source. As one probes closer to the edge of a finite source, the column density along each line of sight approaches zero. Thus,

Table 1. Model Parameters

Parameter	Value
Cloud size [r_{out}]	1.0 pc
Cloud thickness [r_0/r_{out}]	10^{-5}
Cloud opacity [τ_0 at $0.55\mu\text{m}$]	10-300
Density distribution [$n(r)$]	$n_0(r_0/r)^m, m = 0, 1, 2$
Opacity function	$Q_0(\lambda_0/\lambda)^{\beta}, \beta = 1.5$
Luminosity of internal source [L_{*}]	0-300 L_{\odot}

when fitting these outer radii, α is artificially increased. It is possible to relate the theoretical column density to the density power index by

$$N(p) \propto \int (z^2 + p^2)^{-m/2} dz, \quad (17)$$

where p is an impact parameter and z is the distance along the line of sight. For different values of the density distribution index, a column density map is formed. Following Yun and Clemens (1991), by matching the derived column density map with the calculated map, a value of m can be found.

3 THE TESTING PROCEDURE

In order to evaluate the reliability of current semianalytic methods of analysis one must compare the derived source parameters with their true values. As the source parameters for actual observations are not known, we have created simulated observations using a modified version of the 1D radiative transfer code of Egan, Leung & Spagna (1988). The output of these models are treated as observational data and analysed using current techniques to derive the source parameters. These derived results can then be compared with the original model parameters. Any differences between the two sets of data can be attributed to the method of analysis.

3.1 Model parameters

We model sources in the interstellar medium that are predominantly heated externally by the interstellar radiation field. Regions of star formation, such as many dark clouds or Bok globules, are the primary motivation. The processes involved in low-mass star formation are relatively well understood (see e.g. review by Shu, Adams, & Lizano 1987). On the other hand, while the picture is not as complete in the high-mass case (see e.g. Churchwell 1993, 1999), recent work (van der Tak et al. 2000; Doty et al. 2002a) seems to suggest that in general similar scalings may be at least potentially reasonable. In both situations, an understanding of the source parameters (dust properties, material distribution, existence/nature of an embedded star) are important (see e.g., Andre, Ward-Thompson, & Barsony 2000). Typical model parameters are given in Table 1.

In our models, we consider both internal and external heat sources. Externally we use the interstellar radiation field (ISRF) of Mathis, Mezger, & Panagia (1983) as the primary source of heating of the dust grains. We have also considered the effects of an updated ISRF compiled by Evans (2001) for comparison. This results in no significant

qualitative difference in our results. To study the effects of young stellar objects (YSOs), protostars, and other embedded sources, we have also considered embedded sources with luminosities ranging from $0 L_{\odot} \leq L_* \leq 300 L_{\odot}$.

The distribution of material in a star forming region is a topic of continuing study. Both theoretical (e.g., Larson 1969; Shu 1977) and observational (e.g., Fuller & Myers 1993; van der Tak et al. 1999; Evans et al. 2001) studies suggest that the density distribution can be well fit by a power law. On the other hand, recent work (e.g., Henriksen, Andre, & Bontemps 1997; Alves, Lada, & Lada 2001; Whitworth & Ward-Thompson 2001) predict/infer more realistic density profiles, including multiple power laws and Bonner-Ebert spheres. Observations and detailed modeling by Evans et al. (2001) for a number of star-forming sources suggest that it may not always yet be possible to observationally distinguish between power-laws and Bonner-Ebert spheres. As a result, and as we wish to provide a simple yet somewhat realistic parameterization, we restrict our study here to power laws as given in equation (2).

Based upon models for cloud collapse and observations of star-forming regions (e.g., Shu 1977; Whitworth & Summers 1985; Foster & Chevalier 1993; Chandler & Sargent 1993; Ward-Thompson et al. 1994; Andre et al. 1993), we model sources with density distribution indices in the range 0–2, namely $m = 0, 1, \text{ and } 2$. We arbitrarily take the outer shell radius to be $r_{\text{out}} = 1$ pc, and the ratio of the inner and outer radii to be $r_0/r_{\text{out}} = 10^{-5}$. This choice of inner radius is chosen to usually yield dust temperatures of $\sim 1000\text{K}$. We find that the choice of outer radius has little effect on the resulting spectra.

We take the grain opacity function to be a power law of frequency as given in equation (3). Laboratory experiments show that for crystalline grain material, $\beta \approx 2$ and for amorphous grain material, $\beta \approx 1$ (see e.g., Tielens & Allamandola 1987; Henning, Michel, Stognienko 1995; Agladze et al. 1996; Jager, Mutschke, & Henning 1998; Fabian et al. 2001). Cox and Mezger (1989) have shown that for $1 \leq \beta \leq 2$, the general behavior of the opacity function should be covered in our models. Consequently, we take a value of $\beta = 1.5$. We normalized our opacity function to Draine’s (1985) values at $2.2\mu\text{m}$ for the scattering component and at $190\mu\text{m}$ for the absorption component. These grain properties not only generally represent laboratory data, but they also have the advantage that they reproduce observations of at least Orion quite well (Doty & Neufeld 1997).

Typical flux spectra for sources of varying luminosity and density distributions are shown in Fig. 1. In Fig. 2 we show typical temperature distribution for sources of varying luminosity and density distributions.

4 DUST TEMPERATURE

Upon integrating equation (5) over all frequencies, it can be seen that the thermal energy density varies as $T^{4+\beta}$. As a result, a small change in temperature translates into a large change in the emergent spectrum. Therefore, it is very important to determine the temperature distribution (Doty and Leung 1994; Shirley et al. 2000). The effect of different temperature distributions can be seen in Figs. 1 and 2. The peak wavelength of emission as well as the width of the

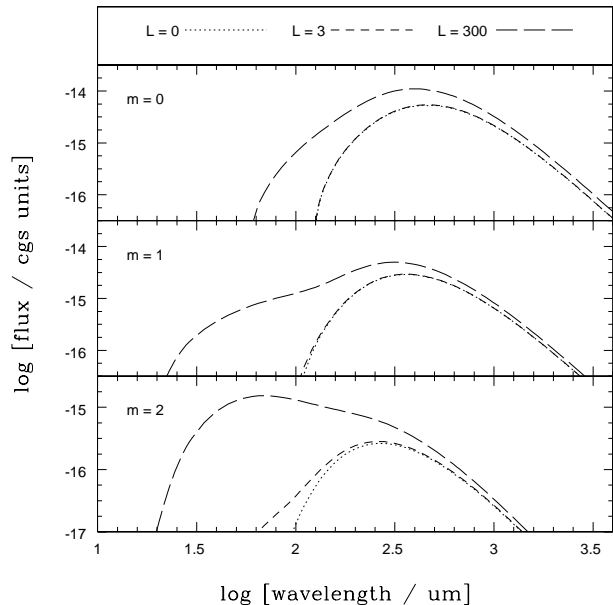


Figure 1. Sample spectra for various models with $\tau_0 = 100$. The three panels correspond to different values of the density distribution index, m . The different line types (dotted, short-dashed, long-dashed) correspond to various values of the central luminosity ($0, 3L_{\odot}, 10L_{\odot}$ respectively). Note the effect of central luminosity on dust temperature, and hence on the short wavelength end of the spectra.

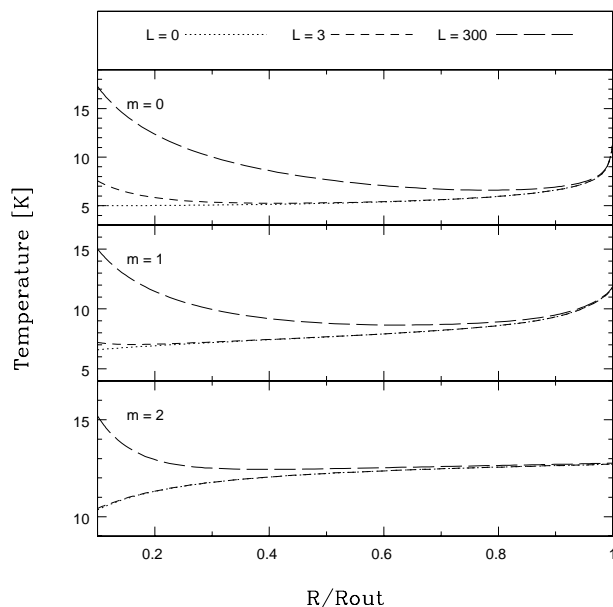


Figure 2. Comparison of dust temperatures as a function of position in the source. The models, lines, and panels are the same as in Fig. 1. Notice how an increase in the internal luminosity leads to higher temperatures in the interior, while the temperature on the outer edge is fixed by the ISRF. Note also the correlation between similar temperature distributions here, and flux spectra in Fig. 1.

spectra are affected by the dust temperature distribution. For the low luminosity embedded sources, the spectrum for the $m = 2$ density distribution peaks at shorter wavelengths than the spectra for models with $m = 1$ and $m = 0$. This is consistent with the corresponding temperature distributions in Fig. 2, where the $m = 2$ models are generally warmer. On the other hand, for the low luminosity embedded sources, the more uniform sources having $m = 0$ and $m = 1$ have a greater range of temperatures, and in general have cooler dust. The range in temperatures results in a wider spectrum in Fig. 1.

This effect is also seen when comparing the models with $L_* = 300L_\odot$ with those of lower luminosity. In this case, the central source heats the dust to 800-1000K on the inner edge, producing a very large range of dust temperatures in the envelope. The highest temperatures occur with increasing optical depth and density distribution index, m , due to radiation trapping in the interior. Conversely, the inner dust temperature for a source with either no or a low luminosity central source is between 5-15 K with the higher temperatures resulting from a lower optical depth and a higher density distribution index, m . These temperatures are not seen in Fig. 2 due to the axes chosen for the plot. The corresponding emission spectra of the high luminosity cases both peak at a higher flux and have emission over a broader range of wavelengths.

4.1 Isothermal approximation

As the intensity along a ray depends upon the temperature-dependent emissivity integrated along the line of sight, it is difficult to determine the temperature distribution in regions of star formation. As a result, it is easiest to assume the source is isothermal. This assumption is best suited for sources which have either no embedded source, or only a very low luminosity central source. As seen in Fig. 2, the temperature distribution is about constant for more than 50 per cent of the source for such cases. When the distribution is not constant, it only changes by 2-5 K. On the other hand, for higher luminosity central sources the range of temperatures is 800-1000 K.

In order to determine the appropriate isothermal temperature to assign to a given source, it is often easiest to consider the peak of the spectrum. We accomplish this using a Wiens Law modified to account for the wavelength dependence of the absorption coefficient, Q_ν .

In general, the peak of the emergent spectrum (I_ν) for an opacity index β can be given by

$$T_{\text{peak}} = \frac{f(\beta)}{\lambda_{\text{peak}}(\mu\text{m})} \text{K}. \quad (18)$$

Here $f(\beta)$ is determined numerically, with results shown in Fig. 3. As can be seen, the results are well-fit by $f(\beta) = 4620e^{-0.2357\beta}$ with a correlation coefficient of $r^2 = 0.9986$ for the range $1 < \beta < 2$. In the case that $\beta = 1.5$ (see Sect. 6 below), we find that $f(\beta) = 3234$. This temperature can then be compared to other physical temperatures associated with the source. In this way it is possible to know what meaning, if any, can be assigned to this forced isothermal temperature.

One temperature used for comparison is the number-weighted grain average temperature defined as

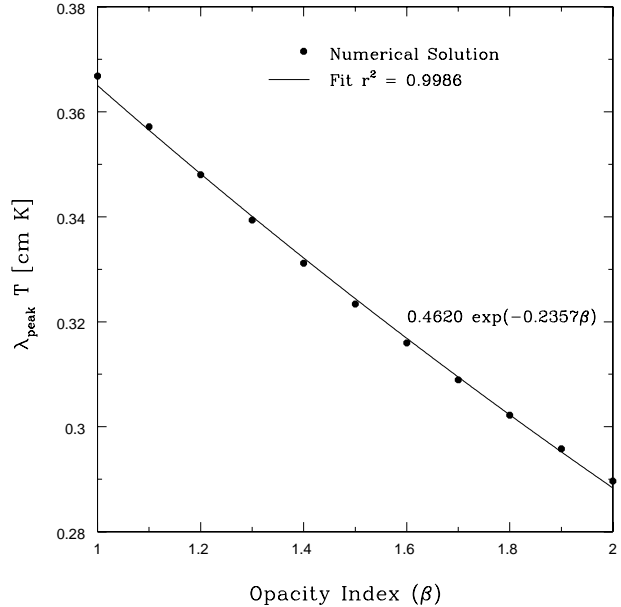


Figure 3. The product of the peak wavelength and source temperature for a Wiens law modified to account for various opacity indices. The numerical results (data points) are plotted as a function of the assumed opacity index. The data are well-fit by the function (solid line) $f(\beta) = 4620e^{-0.2357\beta}$ with a correlation coefficient of $r^2 = 0.9986$.

$$\langle T \rangle_N = \frac{\int T(r)n(r)4\pi r^2 dr}{\int n(r)4\pi r^2 dr}. \quad (19)$$

This temperature is the average grain temperature. Another comparison may be made with the energy-weighted temperature defined as

$$\langle T \rangle_E = \left(\frac{\int [T(r)]^{4+\beta} n(r)4\pi r^2 dr}{\int n(r)4\pi r^2 dr} \right)^{1/(4+\beta)}. \quad (20)$$

Physically, this temperature represents the average energy emitted by a grain.

In all models tested, except $m = 2$, $L_* = 300L_\odot$ as discussed below, the peak temperature inferred from equation (18) does not vary more than 0.5 K from $\langle T \rangle_E$. This can be understood as due to the fact that most of the energy is radiated at a wavelength corresponding to the peak emission and so the corresponding temperature should be about the energy-weighted temperature. Also, the temperature agrees well with $\langle T \rangle_N$. In Fig. 4, we plot $\Delta T \equiv T_{\text{peak}} - \langle T \rangle_N$ as a function of the optical depth of the model for cases of different central luminosity. The one outlying result is the $m = 2$ case with a highly luminous embedded source having $L_* = 300L_\odot$. In this case, the average difference between the inferred and number-weighted dust temperature is about 50K. This difference can be understood by the fact that in a centrally condensed source more dust will be affected by a central heat source. Consequently, the peak of the spectrum is shifted to shorter wavelengths, and is due to the central source rather than by the ISRF. As a result, the inferred temperature from the peak of the flux spectrum is considerably too high and inapplicable to the problem at hand. In all other cases in Fig. 4, the ISRF dominates the majority of the dust heating, and a few trends are immediately obvious.

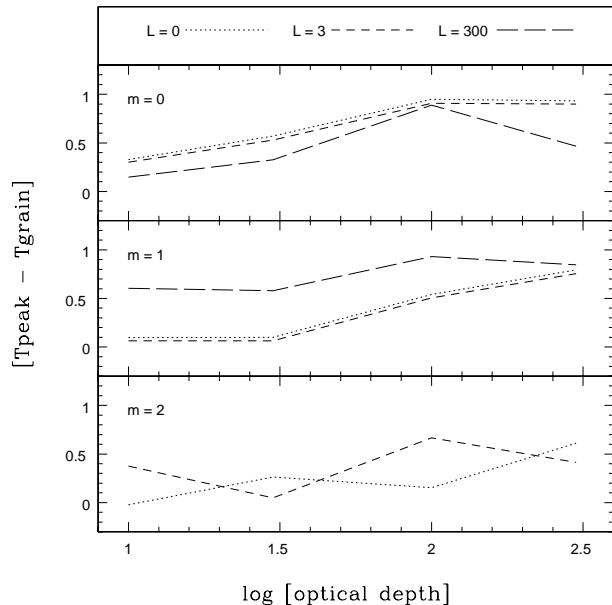


Figure 4. Comparison of the temperature inferred from the peak of the flux spectrum, with the number-weighted average dust temperature for the grid of models previously discussed. Note that the temperature inferred from the peak of the dust spectrum is a good measure of the average (by number) dust temperature, often accurate to within 0.5 K.

As optical depth increases, so does ΔT , although the largest difference is 1 K. For $\tau_0 < 30$ the difference is at most 0.6 K. In conclusion, deriving the dust temperature using a modified Wiens Law will give a temperature that closely relates both the average energy and the average grain temperature.

In order to see the effect of using an isothermal temperature on the emergent spectra, in Fig. 5 we plot both the output spectra and a blackbody modified by the absorption coefficient, normalized at the peak in the left panels. In the right panels we plot the fractional difference between the blackbody spectrum and the actual emergent spectrum. For the longer wavelength portion of the spectrum, the derived blackbody spectrum is at most about 20 per cent in error, with larger discrepancies occurring at a smaller density distribution index, m . The $m = 2$ case is within 10 per cent, and the $m = 1$ case is within 15 per cent. For wavelengths shorter than the peak, the errors tend to get worse. In the $m = 2$ case, the errors reach only about 5 per cent, while for the $m = 1$ and $m = 0$ cases, the errors can reach over 100 per cent. As the luminosity of an embedded source increases, stellar emission makes it difficult to fit the spectrum with a single temperature blackbody. It should be noted that Fig. 5 shows the most favorable case for a single temperature fit, since the lack of any internal heat source makes this the most isothermal of all the models. As a result the other ($L_* \neq 0$) cases will be even more poorly fit by a single temperature.

Although the peak of the output spectrum is a reasonable estimate for either the number- or energy-weighted average dust temperature for regions without strong internal sources, these single temperatures do not represent the actual temperature distribution in the region. As a result, isothermal fits do not generally duplicate the output spectra

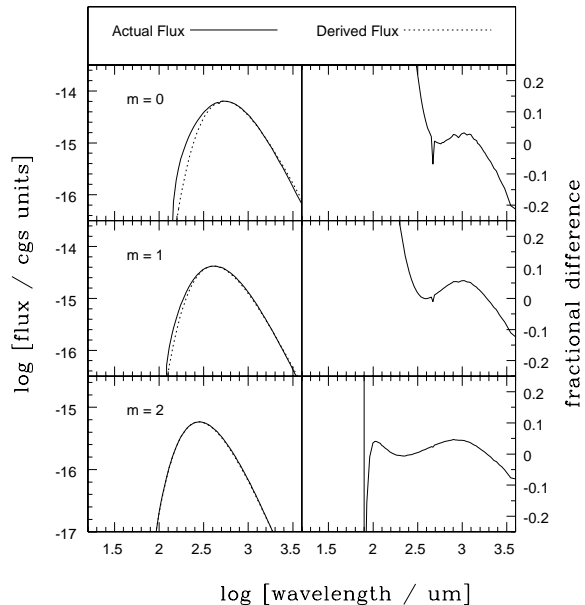


Figure 5. The left hand panels show a comparison between the actual flux spectra (solid lines) and dust-modified blackbody spectra at the temperatures inferred by the modified Wiens law in equation (18) of the text (dashed lines). Results shown here are for $\tau_0 = 100$, and $L_* = 0L_\odot$. Note the good agreement, especially near the peak. For better comparison, the right hand panels show the fractional differences between the spectra. Note that even though a single dust-modified blackbody fits well, the non-isothermal nature of the sources can be clearly seen in the fractional differences.

to better than 10 per cent. Consequently, probes that may be sensitive to the range of dust temperatures in a region may require self-consistent radiative transfer modeling.

5 DUST MASS

If the mass of a single grain is m_g , then the total dust mass is given by

$$M = m_g \int n(r) 4\pi r^2 dr. \quad (21)$$

Knowledge of the density distribution, $n(r)$, is necessary to determine the dust mass exactly, without assumptions. Although the form can be approximated by a power law, its evaluation requires knowledge of both r_0 and n_0 , which are the inner radius and the amount of dust at the inner radius respectively. These quantities are unknown, suggesting the use of more approximate methods based upon dust emission.

5.1 Dust mass from integrated luminosity

The total integrated luminosity measures the total energy emitted per unit time and is given by

$$L = \int L_\nu d\nu. \quad (22)$$

Since dust grains can only emit what they absorb, the total energy emitted should be proportional to the optical depth,

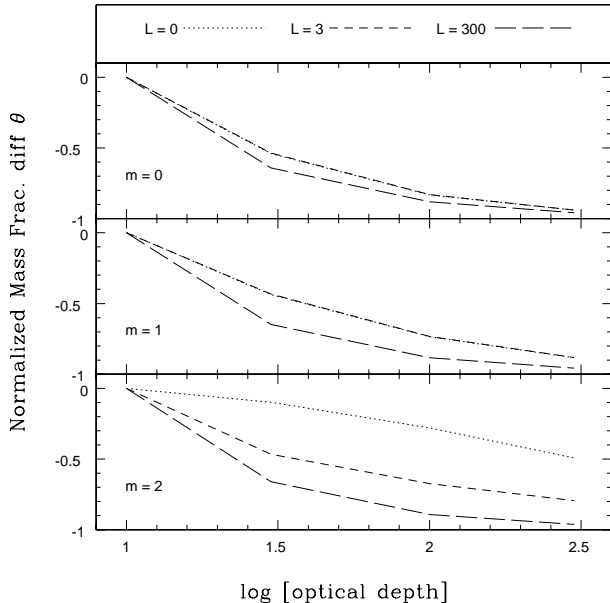


Figure 6. The fractional difference between the dust mass inferred by considering the relative integrated luminosity between sources, and the actual dust mass for the grid of models. The results are normalized at the lowest optical depth. Notice how the estimated dust masses are further in error with increasing optical depth and decreasing density contrast, due to the increasing opaqueness of the sources to radiation from the ISRF.

or dust mass, of the source. A relative mass can therefore be determined by taking the ratio of luminosities of two different sources. The two basic underlying assumptions here is that the sources are optically thin to the radiation of interest and that the two sources being compared share the same temperature distribution. Only then will the dust mass be proportional to the total emitted energy. We test this method by calculating the dust mass for a series of models of increasing optical depth and different central luminosities. We normalize the models to the value at $\tau_0 = 10$. In Fig. 6, we plot the normalized fractional difference in mass, Θ , defined as

$$\Theta \equiv \frac{M_{\text{derived}} - M_{\text{actual}}}{M_{\text{actual}}} \quad (23)$$

for varying optical depths. The dust masses inferred by this method are consistently lower than the actual dust masses for the same sources. The median error is about 50 per cent with errors as great as 96 per cent (i.e. a factor of ~ 100). The discrepancy increases with the optical depth, and plateaus at higher optical depths regardless of the luminosity.

The plateau for $\tau_0 > 100$ is due to the fact that the sources are no longer transparent to most IR radiation. As the optical depth increases a greater percentage of incident energy from the ISRF is absorbed. Eventually, at high enough optical depths, all of the possible radiation will be absorbed leading to a constant total luminosity and hence an inferred mass independent of τ . This effect is less dramatic in the $m = 2$ case because most of the mass is centrally condensed, and therefore only radiation that penetrates to the center of the source will be absorbed.

The consistently lower results can be understood in the following way. The luminosity is proportional to the density distribution times the energy emitted per grain, which is the blackbody function modified by the absorption coefficient. In order for the luminosity to be truly proportional to the optical depth the energy emitted per grain needs to be the same for the two sources being ratioed. However, as the optical depth increases, the ability for radiation to heat the inside of the source attenuates as $e^{-\tau}$, and so the temperature distribution between sources of different optical depths are no longer going to be the same. Therefore, the actual luminosity does not increase as quickly as the luminosities predicted using this method and hence, the results are consistently lower.

For the $m = 2$ case, the differences in the cases with different luminosities can be explained as follows. Most of the mass is located to the inside, and therefore most of the optical depth is located there as well. Therefore, a majority of the source will be optically thin and so the same majority of the source will be heated to a constant temperature. This helps explain why the results for these cases are better than for the $m = 1$ and $m = 0$ cases.

5.2 Dust mass from specific luminosity

Hildebrand (1983) proposed that the dust mass of an optically thin and isothermal source can be related to the observed flux of a given frequency and distance to the source via equation (9). In order to calculate the total dust mass, the mass of a grain, isothermal temperature, and Q_ν need to be calculated or estimated. To alleviate this problem, we take the ratio of dust mass for similar sources. In this way, the only parameter that needs to be estimated is the temperature, which we calculate using the modified Wiens law in equation (18). We use the wavelength of peak emission as the wavelength in equation (9). To evaluate this method we calculate the dust mass for a series of models of increasing optical depths and different central luminosities, and compare them to the actual values. We plot the fractional difference as a function of optical depth in Fig. 7.

The results are quite good. A median error of about 25 per cent is found for $m = 0$, with errors between 10–20 per cent depending on the central luminosity for $m = 1$, and approximately 10 per cent errors for $m = 2$. As the optical depth increases, the differences also tend to increase. As was the case for calculating temperature, the mass inferred in the $m = 2$, $L = 300 L_\odot$ model is a factor of 50 times higher than the actual mass. The error is due to the inability to determine accurately an average temperature of the source.

In most cases, as the luminosity increases, the error increases as well. However, in the case of $m = 1$, $L = 300 L_\odot$ we find that the errors are less than without an embedded star. With a constant density distribution, a larger proportion of the mass is found to the outside of the source and so there is a larger change in temperature to the outside of the source (see Fig. 2). However, when there is an embedded star with a high luminosity, the rest of the source is heated and it causes a smaller change in temperature to the outside of the source, giving the appearance of a more isothermal source (see Figs 2 and 4).

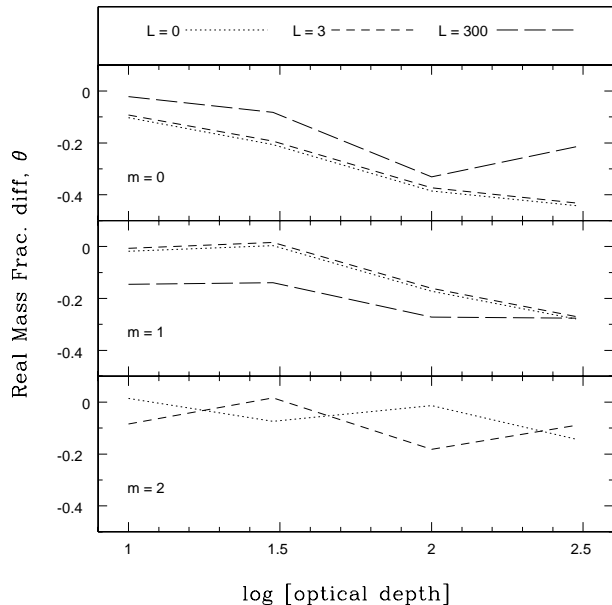


Figure 7. The fractional difference between the mass inferred from the peak of the flux spectrum and the actual mass, for the grid of models discussed previously. Notice the results are generally better than the masses inferred by comparing integrated luminosities. This is related to the quality of the dust temperature from the peak as a measure of the number-weighted dust temperature.

6 OPACITY FUNCTION

The grain opacity index, β , defines the form of the opacity function. The effects are also evident in the flux spectrum. A lower β has the effect of increasing the amount of emission at wavelengths longer than the visible range relative to the emission in the visible. Therefore, a lower optical index will broaden the spectrum. Conversely, a higher β has the effect of narrowing the spectrum.

6.1 Finding β as a ratio of luminosities

A more common, and potentially easier method for determining β is to use the ratios of luminosities from two different wavelengths, as shown in equation (12). This method relies on two assumptions: that the RJA holds, and that the source is optically thin. Again, we have evaluated this technique for models of increasing optical depths and different luminosities. Fig. 8 shows the opacity index derived between a reference wavelength, denoted by the various symbols, and a variety of longer wavelengths. Our results are consistently lower than the actual value but asymptotically approach it for longer wavelengths. The source is still optically thin over the wavelength range we are looking (at $650\mu\text{m}$, $\tau = 0.002$) and so the deviations are due to the RJA. The presence of a temperature distribution has the effect of adding up multiple blackbodies. The RJA will only hold true if we are on the long wavelength end of a blackbody corresponding to the coolest dust. For the coolest dust in our models (~ 5 K), the shortest wavelength that satisfies the RJA is $\sim 2800\mu\text{m}$.

As can be clearly seen in Fig. 8, there is some wavelength short of which the inferred opacity indices are inap-

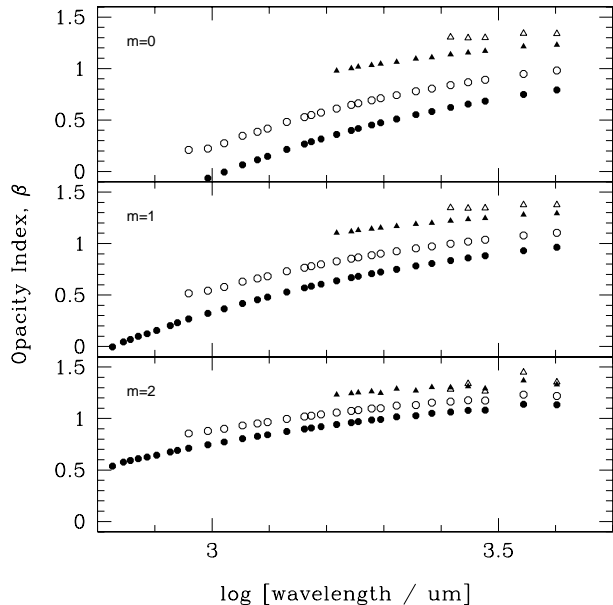


Figure 8. The inferred dust opacity index for models with $\tau_0 = 300$. The results for other optical depths are qualitatively similar. The opacity indices are derived from the slope of the FIR spectrum, and plotted versus the shortest wavelength of the wavelength-pair used in the slope determination. Like-symbols correspond to variations in the longer wavelength of the pair. Note that even for wavelengths at which the source is transparent, one must go to extremely long wavelengths to ensure that the RJA holds.

plicable. We call this wavelength the cutoff wavelength, and define it to be the shortest wavelength in the pair used in equation (12) for which β is determined to within 20 per cent. In Fig. 9, we plot λ_{cutoff} as a function of optical depth for the models considered. We see that in general, wavelengths greater than $1000 - 2000\mu\text{m}$ should be used in determining β from the slope of the FIR spectrum, so long as the dust continuum dominates the free-free emission – a significant problem in some sources. These results can be considered a means of inferring the validity of the RJA.

6.2 Fitting the spectrum to determine β

The opacity index may also be determined by treating it as a fitting parameter while fitting the spectrum. It is easiest and somewhat common (see e.g., McCarthy, Forrest, & Houck 1978; Sopka et al. 1985) to assume an isothermal source in making these fits. While this makes the fitting easier, it also removes the effect that the temperature distribution has on the width of the spectrum. Consequently, the derived opacity indices are artificially raised to compensate. To try and alleviate this problem, we have only fit the longer wavelength end of the spectrum as it should be more optically thin, as well as sample the cooler (and hence more isothermal) dust. This can be seen in Fig. 1 where we see that a star does not have a significant effect on the presence of the spectrum at longer wavelengths.

Based upon this reasoning, and with the advent of recent and upcoming far IR/submm observational data (e.g.

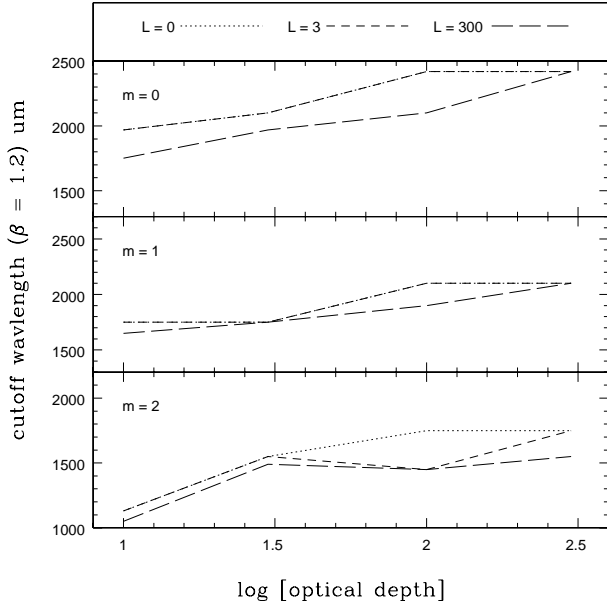


Figure 9. The variation in the cutoff wavelength with optical depth for the models considered. As discussed in the text, the cutoff wavelength is the shortest wavelength for which the slope of the FIR will yield an opacity index correct to within 20 per cent

SCUBA, SIRTf, Herschel, etc.) we fit the wavelength range $500\mu\text{m} < \lambda < 900\mu\text{m}$ for models of different density distributions and increasing optical depth shown in Table 1. Our results are shown in Fig. 10. The errors in this method range from 0 to 60 per cent. In the case of $m = 1$ and 2, the derived indices are too high, with slightly better results as the optical depth increases. For the $m = 0$ case, the derived indices are too high by about 7 per cent for optical depths $\tau_0 < 30$, and at an optical depth of $\tau_0 = 300$ the derived indices are too low by 15 per cent.

For luminosities $L < 3L_\odot$, the derived opacities follow the same trend as the starless core models. But for luminosities $L > 3L_\odot$, the derived opacity indices tend to be lower, and more accurate by an average of 50 per cent. Even at $500\mu\text{m}$, the star affects the spectrum noticeably (see Fig. 1). The spectrum is artificially broadened by the star, and thus the derived opacities are lowered. In effect, the errors caused by the isothermal assumption are counteracted by the extra luminosity from an embedded star.

In order to account for the non-isothermal nature of the sources, we also fit the spectrum with two blackbodies. This simulates a two-temperature 'core-halo' model, with a warm exterior shell heated by the ISRF, and a cool interior shell. These fits reduced our error to a maximum of 7 per cent. However, the five fitting parameters make it more difficult to obtain reasonable results due to the presence of local minima, with the accuracy of the fitting depending more significantly on the initial guess for the parameters. In this case, the fits have a maximum error of 0.1 in β , with most having errors of 0.05 or less, representing a median error of ~ 3 per cent.

We also considered the use of different wavelength ranges on the derived opacity indices. We did not test the

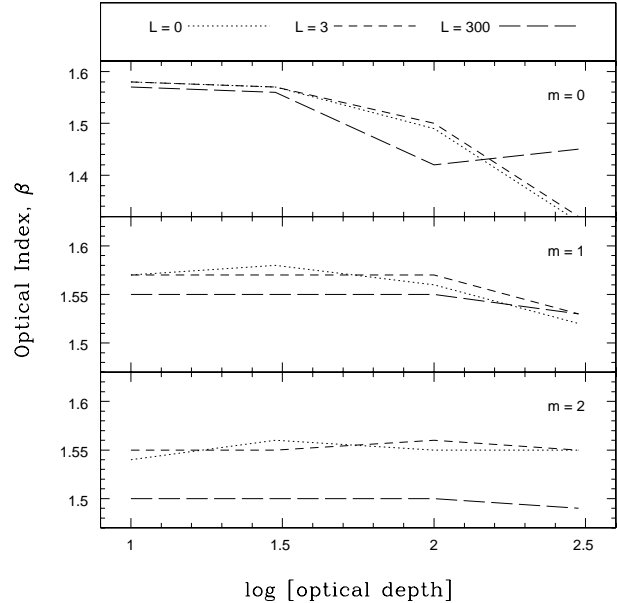


Figure 10. The dust opacity index inferred by fitting the dust spectrum for the grid of models considered. The results are much better than those inferred from the slope of the FIR spectrum, and are often good to better than 10 per cent.

use of shorter wavelengths, due to contamination of the spectrum by the embedded sources. Using the range from $500\mu\text{m}$ to the end of the spectrum (about $3000\mu\text{m}$), the derived indices are uniformly low for a single blackbody fit, with an average $\beta = 1.2$. This effect is due to the addition of emission from the coolest dust, which causes the spectrum to broaden past $900\mu\text{m}$. Therefore, even when longer wavelengths are chosen, the results are not appreciably better, as multiple temperatures are still sampled.

7 DENSITY DISTRIBUTION

The density distribution is crucial to our understanding of the processes and regions of star formation. Both observations and theory indicate that typical distributions can be well-described by a power law. As a result we assume a power law distribution in all of our models. The density index, m , helps to determine the emergent radiation of a source. A centrally condensed source ($m = 2$) is less affected by the ISRF and more affected by embedded sources. In contrast, a constant distribution ($m = 0$) is affected by the ISRF more than by an embedded star (see Fig. 1).

7.1 Density distribution in a resolved source

Yun and Clemens (1991) extended a note by Tomita et al. (1979) regarding the relationship of the column density power index to the density distribution power index. Using equation (17), a column density map can be formed from the density distribution index. By matching the derived and calculated column density profiles m can be constrained.

To test the reliability of this method we have calculated the density distribution index for a series of models

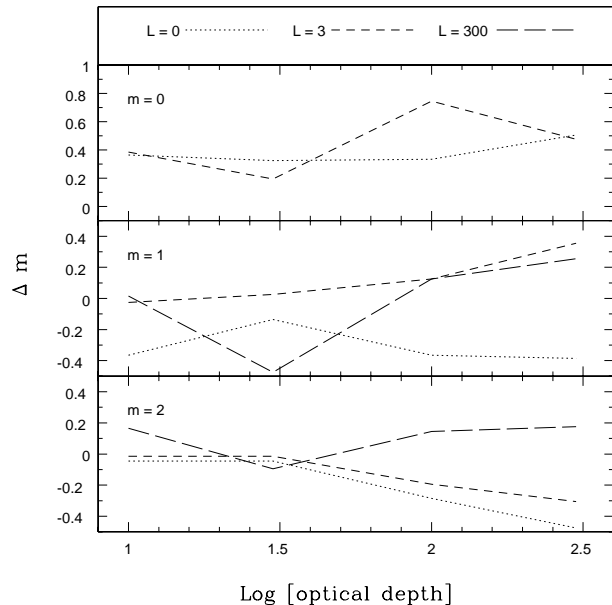


Figure 11. The difference between the inferred and actual dust density distribution for the grid of models considered. Notice that the results are better for more centrally-condensed sources.

with different density distributions, optical depths, and central luminosities. We consider the wavelengths of $175\mu\text{m}$ and $215\mu\text{m}$, as they should be near the peak of emission. As the effects of beamsizes are instrument-dependent, and may potentially confuse the analysis, we consider an infinitely small pencil beam for most of this work in order to keep the possible sources of uncertainty to a minimum.

Based upon the difficulty in determining an ‘edge’ to the source, and based upon our experience in these fits, we find that choosing impact parameters in the range $0.03 r_{\text{out}} < p < 0.3 r_{\text{out}}$ provide the optimal fits over a wide range of source parameters. We also tested different impact parameters, both closer to the center, and out towards the edge. We found that both of these cases gave poor results. As the beam probes closer to the edge, part of the beam is off the source. As a result there is an artificial lowering in the calculation of the column density. As the beam probes toward the center, the contamination of the spectrum by the embedded source yields poor results.

In Fig. 11, we plot $\Delta m \equiv m_{\text{calculated}} - m_{\text{actual}}$ for the conditions discussed above. We find that the results are moderate at best. We find a median $|\Delta m|$ of $0.1 - 0.4$, which corresponds to a difference from as low as 5 per cent to over 100 per cent. The maximum deviations range between 0.5 and 0.8, corresponding to fractional differences between 25 per cent to over 100 per cent.

In the $m = 2$ case, we see that the results are good for the low luminosities and optical depths. This is due to the fact that the source is fairly isothermal in these cases. As the optical depth increases, the inferred density distribution index also tends to worsen. This is because at higher optical depths, the temperature gradient is larger. The problem is not due to the optical depth because the source is transparent at these wavelengths. For the high luminosity case, we find that the values are not as good as the low luminosity

cases at low optical depths, but tend to be slightly better as optical depth increases. We find that generally $\Delta m > 0$, meaning that the inferred index is greater than the actual index. This is because we see a slight increase in temperature towards the center and so we get more emission at smaller radii. As a result, we infer more mass towards the center, giving us a larger distribution index.

We find that the $m = 1$ case is harder to understand. We find that for no embedded star that there is a monotonic decrease in temperature. As a result we have more inferred mass towards the outside, artificially lowering the index.

In the $m = 0$ case, the results are uniformly too high with a median difference of 0.4. The high luminosity case did not produce any results.

For comparison, we have also tested the effects of using longer wavelengths of $670\mu\text{m}$ and $800\mu\text{m}$, for comparison with general wavelength ranges probed by SCUBA and other recent observations. We find that using these wavelengths results in somewhat worse results. In particular, the resulting mean differences between the density distribution indices inferred at these longer wavelengths and those inferred near the peak of the spectrum are 6, 15, and 20 per cent for $m = 0, 1, 2$ respectively. In all cases, the indices inferred near the peak of the flux spectrum provide more accurate results.

We also tested the effects of different beam sizes by varying the beam size from 15 arcsec to 4 arcmin (roughly from SCUBA to IRAS beam sizes), corresponding to roughly 60 and 4 beams across the source respectively at an assumed distance of 500 pc. We find that the effect of beam size is relatively small for smaller beams. In particular, for beams approximately appropriate for SOFIA (~ 6 arcsec) and SCUBA (~ 15 arcsec), the inferred density distribution has a median variation from the infinitesimal beamsizes of only ~ 5 per cent. Larger beams, such as $\sim 4'$ similar to IRAS produce results with at least a 70 per cent difference. In both cases, these results are due to the ability to resolve the source, and the effect of the source only partially filling the beam for pointings near the edge. As a result, it appears that for regions with small temperature gradients, relatively well-resolved observations provide results that are rather insensitive to the beam size.

7.2 Detailed modeling of the flux spectrum to find the density distribution

Another approach to try and help determine the density distribution is to model the flux spectrum. In order to test this method we produced artificial observations for a base model similar to that described in Sect. 3, but having $m = 1.5$ to simulate a more ‘intermediate’ value. In order to more closely resemble actual observations, we randomly added noise to the simulated spectra. The noise amplitude was as large as 25 per cent of the simulated observations, with a median noise of 13 per cent over the entire spectrum. We then ran over 2000 models that bracketed this base model in two parameters, optical depth and density distribution index. Based upon the results of Sect. 6, we assume that the grain properties could be determined relatively accurately, and thus treat β as known.

We evaluated the models by calculating the chi-squared difference between the flux spectrum of the test models with

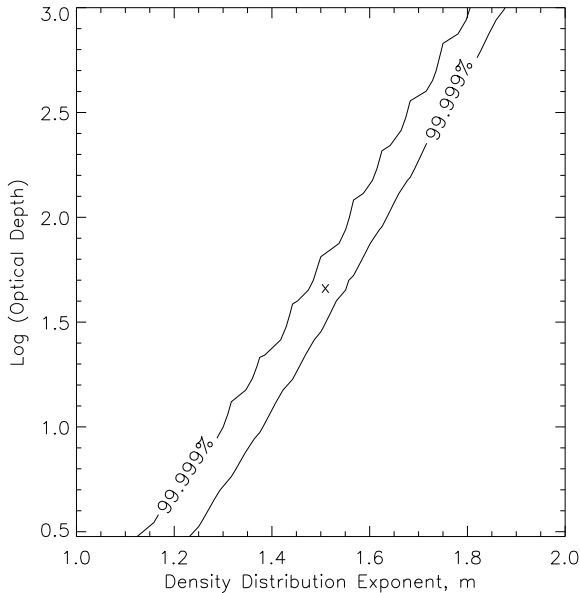


Figure 12. A plot of the 99.999 per cent confidence contour in the determination of the density distribution exponent as a function of the optical depth of the source. While there is a definite line of degeneracy, uncertainties in the optical depth of an order of magnitude yield uncertainties in the density distribution exponent of only 0.25 – or about 15 per cent.

the simulated observations. In Fig. 12, we plot the 99.999 per cent confidence interval for this result. We can see that for any reasonably constrained optical depth, the density distribution index, m , is constrained to the range $1.2 \leq m \leq 1.8$, which is a difference of 20 per cent from the value of $m = 1.5$ adopted in the model. However, if the optical depth can be determined to within 10 per cent, the error in determining the density index, m , becomes ~ 7 per cent.

Uncertainties of a similar magnitude in m (i.e. $\Delta m \sim 0.2 - 0.3$) can also result from uncertainties in the ISRF (Young & Evans 2002), the source geometry (Doty et al. 2002b), and the assumed value of β . However, it may be possible to constrain these parameters by other data (e.g., bolometric luminosity for pre-protostellar cores, source morphology, and the results of Sect. 6). It is interesting to note that even when these parameters are not well constrained, the uncertainties in m are on the order of the uncertainties implied by the optical depth alone, and smaller otherwise.

7.3 Surface brightness profile

Finally, as the smaller beamsizes of recent and upcoming instruments make it increasingly possible to spatially resolve star-forming regions (see e.g., Evans et al. 2001) it is interesting to consider the implications of the expected surface brightness across the source. Shirley et al. (2000) presented models of the normalized intensity profile as a function of impact parameter for semi-analytic cases similar to equation (17) with various assumptions regarding the temperature profile in the dust envelope. They found that the assumptions of isothermality and the RJA could be important.

For comparison, in Fig. 13 we plot the expected surface

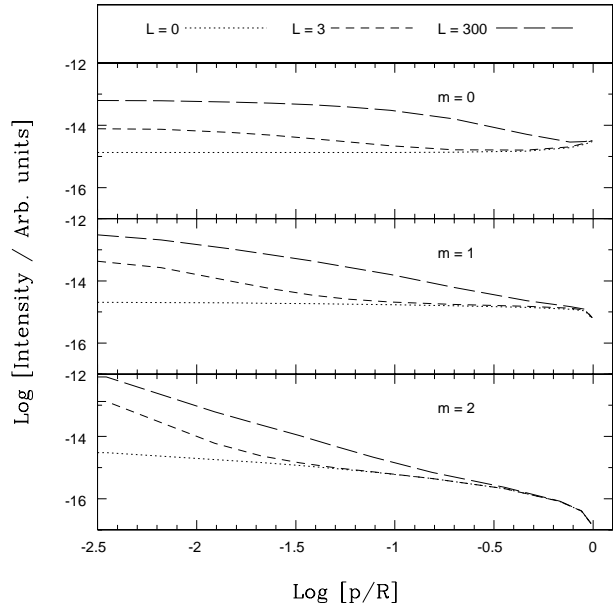


Figure 13. The surface brightness for a pencil beam at $345\mu\text{m}$ across the model sources as a function of impact parameter. All results shown are for $\tau_0 = 100$, with only qualitative differences for other optical depths. The different line types correspond to varying central luminosities, and the panels to different density distribution exponents. Note the effects that both the central source and density distribution have on the surface brightness, suggesting the need for detailed modeling to best interpret such observations.

brightness at $345\mu\text{m}$ as a function of impact parameter for $m = 0, 1, 2$, and $L_* = 0, 3, 300L_\odot$. This wavelength is chosen as it should be near the peak of the source spectrum, and is observable by SCUBA. These results are based upon detailed modeling as described earlier. In this case the dust temperature distribution is determined self-consistently, and the RJA is not applied.

From these results, some conclusions may be drawn. First, for well-resolved sources, it appears that it is possible to infer the dust density distribution index, m . This is especially true if the source luminosity is somewhat constrained, and more importantly if good signal-to-noise data exist near the source edge without contamination from beam dilution, etc. Second, it may be possible to infer the existence of an internal heat source from the surface brightness distribution. This is a problem which is the subject of an upcoming paper (Doty & Moore 2002). Finally, these results show an apparently wider variation in surface brightness across the source than those from approximate methods (see e.g., Fig. 13 of Shirley et al. 2000). The differences are due to the discrepancies between the assumed dust temperature distribution in the approximate methods, and the self-consistent distribution determined through the modeling. This underscores the importance of detailed modeling of emergent radiation for these and any other but the most simple star-forming regions.

8 CONCLUSIONS

We have critically evaluated current semi-analytical methods in analysing regions of low-mass star-formation. In particular, we have investigated the validity of the underlying assumptions for the methods and determined the conditions under which these methods are reliable. Based upon this work, we find that:

1. The temperature distribution plays a significant role in determining the spectrum of a source. As there are no current semi-analytic methods for determining the temperature distribution explicitly, a common assumption is that these sources are isothermal. Although an isothermal temperature with some physical basis can be found using a modified Wiens Law (Fig. 3 and equation [18]), using this temperature does not accurately determine the other source parameters (See Sections 4, 5, and 6).

2. It is difficult to reliably determine the total dust mass without an accurate estimate of grain properties, density distribution, and the distance to the source (Section 5). However, a ratio of mass from two similar sources can be determined using the observed flux at a given frequency. The dust masses determined by this method are accurate to within 50 per cent for all cases where the estimated temperature is in reasonable agreement (5 K) with the average grain temperature – namely for regions with no or weak internal sources. It is also possible to determine a ratio of dust masses using the integrated luminosity. This method is only applicable for low optical depths, as errors approach 100 per cent for $\tau_0 \geq 100$.

3. For an optically thin source and in a region of frequencies where the Rayleigh Jeans approximation holds, the opacity index, β , can be determined using the ratio of two different frequencies as in equation (12). In order to determine the opacity index to within 20 per cent for all optical depths, the pair of wavelengths used need to be longer than about $2500\mu\text{m}$, due to the failure of the RJA and the lack of isothermality of the source. This may be problematic due to the existence of free-free emission which may dominate the thermal dust continuum for some sources. Another method for determining the opacity index is by fitting the spectrum. With a single blackbody fit, β can be determined to within 60 per cent for all cases. If, instead, a two temperature fit is used, the results for β are improved considerably, with a maximum error of only 7 per cent.

4. The density distribution index, m , can be determined for a resolved source that is isothermal along any line of sight by using the ratio of intensities at two different wavelengths. For a theoretically small pencil beam, the results have an error of up to 100 per cent. Errors increase as the beam size gets larger, growing dramatically for pointings in which the source does not fill the beam. The errors also increase somewhat as the wavelengths used decrease. Finally, due to the isothermal assumption, it is important to probe impact parameters that are neither too close to the edge of the source nor too close to the core. We find $0.03r_{\text{out}} < p < 0.3r_{\text{out}}$ works well in the cases studied here.

5. It should be possible to infer the dust density distribution, m , from the surface brightness distribution across the source. This, however, requires good signal-to-noise data toward the source edge. The range in surface brightness distributions is due to the differences in the actual tempera-

ture distributions in the sources, highlighting the need for self-consistent modeling to ensure proper interpretation of observational data.

ACKNOWLEDGEMENTS

We are grateful to the referee, Derek Ward-Thompson, for helpful suggestions, and to Neal Evans for discussions and useful comments. We thank Ewine van Dishoeck for hospitality at Leiden University where the work was initially begun. This work was partially supported under a grant from The Research Corporation, a bezoekerbeurs from the Netherlands Organization for Scientific Research (NWO), and supplementary support from the Battelle Corporation through Denison University.

REFERENCES

- Abraham, P., et al. 2000, *A&A*, 354, 965
Agladze, N. I., et al. 1996, *ApJ*, 462, 1026
Alves, J. F., Lada, C. J., & Lada, E. A. 2001, *Nature*, 409, 159
Andre, P., Ward-Thompson, D., & Molte, F. 1996, *A&A*, 314, 625
Andre, P., Ward-Thompson, D., & Barsony, M. 1993, *ApJ*, 406, 122
Andre, P., Ward-Thompson, D., & Barsony, M. 2000, in: *Protostars and Planets IV*, eds. V. Mannings, A. Boss, & S. Russell (Tucson: Univ. of Arizona Press), 59
Butner, H. M., Evans II, N. J., Lester, D. F., Levreault, R. M., & Strom, S. E. 1991, *ApJ*, 376, 636
Chandler, C. J., & Sargent, A. I. 1993, *ApJ*, 414, 129
Churchwell, E. B. 1993, in: *ASP Conf. Ser. 35, Massive Stars, Their Lives in the Intestellar Medium*, eds. J. P. Cassinelli & E. B. Churchwell, ASP, 35
Churchwell, E. B. 1999, in: *The Physics of Star Formation and Early Stellar Evolution II*, eds. C. J. Lada & N. D. Kylafis, Kluwer, 515
Cox, P., & Mezger, P. G., 1989, *ARA&A*, 1, 49
Doty, S. D., & Leung, C. M. 1994, *ApJ*, 424, 729
Doty, S. D., & Neufeld, D. A. 1997, *ApJ*, 489, 122
Doty, S. D., van Dishoeck, E. F., van der Tak, F. F. S., & Boonman, A. M. S. 2002a, *A&A*, in press
Doty, S. D., et al. 2002b, in preparation
Doty, S. D., & Moore, M. M. 2002, in preparation
Draine, B. T. 1985, *ApJS*, 57, 587
Egan, M. P., Leung, C. M., & Spagna, G. F., Jr. 1988, *Comput. Phys. Comm.*, 48, 271
Evans II, N. J., Rawlings, J. M. C., Shirley, Y. L., & Mundy, L. G. 2001, *ApJ*, 557, 193
Fabian, D., et al. 2001, *A&A*, 378, 228
Foster, P. N., & Chevalier, R. A. 1993, *ApJ*, 416, 363
Fuller, G. A., & Myers, P. C. 1993, *ApJ*, 418, 273
Grady, C. A., et al. 2001, *AJ*, 122, 3396
Helou, G. 1989, in *IAU Symp. 135, Interstellar Dust*, ed. L. J. Allamandola & A. G. G. M. Tielens (Dordrecht: Reidel), 285
Henriksen, R., Andre, P., & Bontemps, S. 1997, *A&A*, 323, 549
Henning, Th., et al. 2000, *A&A*, 364, 613
Henning, Th., Michel, B., & Stognienko, R. 1995, *Planet. Space Sci.*, 43, 1333
Hildebrand, R. H. 1983, *QJRAS*, 24, 267
Ivezic, Z., Nenkova, M., & Elitzur, M. 1999, *User Manual for DUSTY*, Univ. Kentucky Internal Rep.
Jager, C., Mutschke, H., & Henning, Th. 1998, *A&A*, 332, 291
Kerton, C. R., Martin, P. G., Johnstone, D., & Ballantyne, D. R. 2001, *ApJ*, 552, 601

- Krügel, E., Siebenmorgen, R., Zota, V., & Chini, R. 1998, *A&A*, 331, L9
- Larson, R. B. 1969, *MNRAS*, 145, 271
- Launhardt, R., et al. 1996, *A&A*, 312, 569
- Launhardt, R., Ward-Thompson, D., & Henning, Th. 1997, *MNRAS*, 288, L45
- McCarthy, J. F., Forrest, W. J., & Houck, J. R. 1978, *ApJ*, 224, 109
- Men'shchikov, A. B., & Henning, Th. 1997, *A&A*, 318, 879
- Schmid-Bergk, J., & Scholz, M. 1976, *A&A*, 51, 209
- Shirley, Y. L., Evans II, N. J., Rawlings, J. C., & Gregersen, E. M. 2000, *ApJS*, 131, 249
- Shu, F. H. 1977, *ApJ*, 214, 488
- Shu, F. H., Adams, F. C., & Lizano, S. 1987, *ARA&A*, 25, 23
- Siebenmorgen, R., Krügel, E., & Chini, R. 1999, *A&A*, 351, 495
- Sopka, R. J., et al. 1985, *ApJ*, 294, 242
- Tielens, A. G. G. M., & Allamandola, L. J. 1987, in *Interstellar Processes*, ed. D. J. Hollenbach & H. A. Thronson, Jr. (Dordrecht: Reidel), 397
- van der Tak, F. F. S., et al. 1999, *ApJ*, 522, 991
- van der Tak, F. F. S., et al. 2000, *ApJ*, 537, 283
- Visser, A. E., Richer, J. S., Chandler, C. J., & Padman, R. 1998, *MNRAS*, 301, 585
- Voshchinnikov, N. V., & Krügel, E. 1999, *A&A*, 352, 508
- Ward-Thompson, D., Scott, P. F., Hills, R. E., & Andre, P. 1994, *MNRAS*, 268, 276
- Ward-Thompson, D., Zylka, R., Mezger, P. G., & Sievers, A. W. 2000, *A&A*, 355, 1122
- Whitworth, A., & Summers, D. 1985, *MNRAS*, 214, 1
- Whitworth, A. P., & Ward-Thompson, D. 2001, *ApJ*, 547, 317
- Young, C., & Evans, N. J. 2002, *ApJ*, submitted